Photoexcitation and Auger decay of the Renner-Teller split C $1s^{-1}$ π_u^* state in CO_2

E. Kukk,[1,2] J. D. Bozek,[2] and N. Berrah[1]
[1]*Department of Physics, Western Michigan University, Kalamazoo, Michigan 49008-5151*
[2]*Lawrence Berkeley National Laboratory, University of California, Berkeley, California 94720*
(Received 10 December 1999; published 15 August 2000)

The broad ($\approx$700 meV) C $1s \rightarrow \pi_u^*$ resonance in the absorption spectrum of CO_2 has been decomposed into contributions from two Renner-Teller split core-excited states with bent and linear equilibrium geometries using resonant Auger spectroscopy. The C $1s^{-1}$ π^* excited state was found to decay primarily via participator Auger transitions to the $A\,^2\Pi_u$ state of CO_2^+. Analysis of the vibrational structure in the high-resolution Auger spectra, measured at several photon energies across the broad C $1s \rightarrow \pi_u^*$ resonance, was accomplished using calculated Franck-Condon factors for the electronic excitation and de-excitation processes. Estimations of the geometries of the Renner-Teller split core-excited states were obtained from a comparison of the calculations with the resonant Auger spectra. Transitions to the bent core-excited state were found to contribute to the absorption profile exclusively at the photon energies below the maximum of the C $1s \rightarrow \pi_u^*$ resonance, whereas the linear core-excited state becomes accessible at higher photon energies. The symmetric stretch vibrational progression of the linear core-excited state was identified and assigned. The minimum of the potential energy surface of the C $1s^{-1}\pi^*$ core-excited state at its linear configuration was estimated to be 290.4 eV above the ground vibrational level of the ground electronic state of CO_2.

PACS number(s): 33.80.Eh, 33.20.Tp, 82.80.Pv

I. INTRODUCTION

Molecular inner-shell photoabsorption spectra usually exhibit prominent pre-edge structures due to the excitation of core electrons to unoccupied molecular orbitals. Core excitations in diatomic molecules usually give rise to peaks with well resolved vibrational progressions, such as the case of CO [1–3]. Similar transitions in the photoabsorption or electron energy loss spectra of triatomic and larger molecules are often unresolved and considerably more difficult to interpret, mainly because of the larger number of vibrational modes that can be excited. In the case of CO_2, for example, the symmetric stretch (υ_1), bend (υ_2), and asymmetric stretch (υ_3) vibrational modes are to be considered. Excitation of the carbon $1s$ electrons of CO_2 to the π_u^* molecular orbital gives rise to a broad peak in the absorption spectrum, with no resolved vibrational structure [1,4]. Consequently, it is not possible to study in detail the vibronic excitations of the C $1s \rightarrow \pi_u^*$ transitions in the photoabsorption spectrum and characterize the potential energy surfaces of the $1s^{-1}$ π_u^* state.

A qualitative understanding of the core-excited states in molecules can be gained from the $Z+1$ model, since the excited core electron is essentially added to the valence electronic structure of the molecule and the core hole approximates the increased nuclear charge of the $Z+1$ atom. The $Z+1$ analogy for the C $1s^{-1}$ π_u^* state of CO_2 is the ground electronic state of the NO_2 molecule. It is well known that the lowest energy configuration of NO_2 has a bent equilibrium geometry with a 134° O-N-O bond angle and forms a Renner-Teller split pair with a higher-energy linear state [5]. The Renner-Teller splitting removes the twofold degeneracy of the π orbital upon bending of the molecule [6,7]. It is reasonable to assume that the C $1s^{-1}$ π_u^* state of CO_2 is also separated by Renner-Teller splitting into two states, as shown in Fig. 1 [4]. The lower-energy state has a bent equilibrium geometry and is realized in the case of excitations to the π^* orbitals that lay in the bending plane of the molecule (π_{in}^*). The higher-energy linear state is formed by excitations to the out-of-plane (π_{out}^*) orbitals. The π_{in}^* and π_{out}^* orbitals correspond to the a_1 and b_1 orbitals in C_{2v} symmetry, and according to this notation the bent and linear states are labeled A_1 and B_1 in this study, respectively.

Recent experiments measuring angle-resolved ion yield spectra following core-excitation and molecular dissociation, have been able to partially resolve the underlying structure of the C $1s \rightarrow \pi_u^*$ absorption peak [8]. Such experiments are able to distinguish between the excitations to the bent and linear states, but not to resolve any vibrational structure on

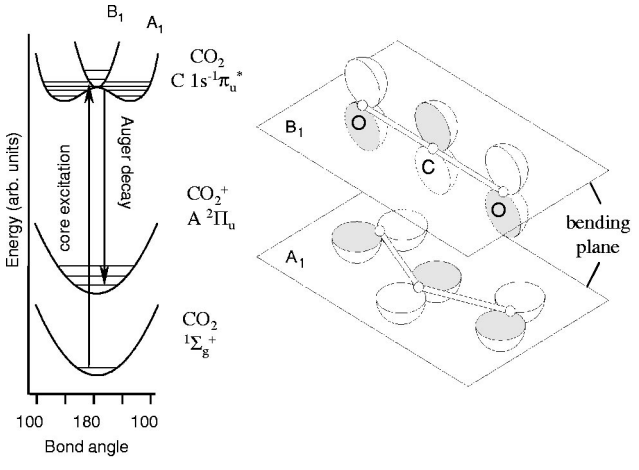

FIG. 1. A schematic representation of the electronic states involved in the core-excitation and Auger decay, showing the potential energy curves along the bond angle of the molecule. The geometry of the π_u^* orbital of the excited electron in the C $1s^{-1}$ π_u^* state is shown to the right.

the C $1s^{-1}\pi^*$ peak. Electron-ion coincidence experiments provide an alternative method for studying the dynamics of the core-excitation process, as demonstrated by recent measurements [9], where the production of the ionic fragments of molecular dissociation was seen to undergo dramatic changes when the photon energy of the excitation was tuned to different regions of the C $1s \rightarrow \pi_u^*$ resonance peak. These effects were shown to relate directly to the changes in molecular summetry during the core excitation and to the excitation of different vibrational modes. The study demonstrated that the vibrational excitations during the C $1s \rightarrow \pi_u^*$ transitions are strongly photon energy dependent.

Core-excited states decay mainly by the resonant Auger process, which can be generally divided into spectator and participator transitions. The former populate two-hole, one-excited-electron final ionic states that are inaccessible by direct photoemission but can only be reached by weak satellite transitions. The participator transitions (autoionization) lead to single-hole ionic states that appear also in nonresonant valence photoelectron spectra. Consequently, the nuclear geometries of these final states are well known, which makes it possible to use the participator Auger electron spectra to characterize the potential energy surfaces of the intermediate core-excited states. The aim of this paper is to study the vibrational structure of the participator Auger spectra of the decay of the C $1s^{-1}\ \pi_u^*$ core-excited state as a function of photon energy by means of high-resolution electron spectroscopy. Such a study yields selective information about different regions of the core-excited state, that are unresolved in the broad photoabsorption peak. This allows one to probe the potential energy surfaces of the two Renner-Teller split states A_1 and B_1 and, furthermore, to assess the vibrational excitations that occur during the carbon $1s$ photoexcitation process.

II. EXPERIMENT

The experiment was performed at the Advanced Light Source at Beamline 9.0.1. Soft x-ray radiation generated by a 10 cm period, 4.55 m long undulator was monochromatized by a spherical grating monochromator (SGM) using a grating of 2100 lines/mm groove density. Total ion yield spectra were measured using a gas cell into which the photon beam entered through a 1000 Å thick Al window. The pressure of the target gas was 1–2 Torr. The ion current was detected from two 15 cm long electrodes placed at both sides of the gas cell. An apparatus based on a Scienta SES-200 hemispherical energy analyzer was used for measuring the electron spectra [10]. The target gas was introduced into a gas cell with differentially pumped openings for the photon beam. The end station is separated from the UHV of the beamline by several differential pumping stages, permitting the use of sample gas pressures up to 10^{-2} Torr within the gas cell. In order to utilize the high resolution of the analyzer in full, the gas cell is equipped with electrodes to compensate for surface potential gradients [11].

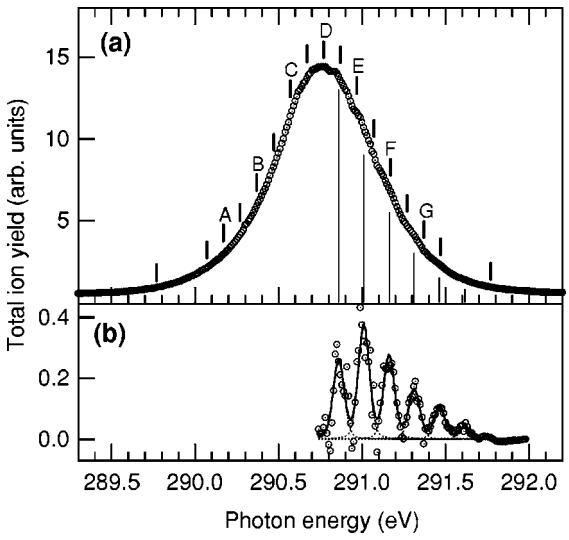

FIG. 2. (a) Total ion yield spectrum over the carbon $1s \rightarrow \pi_u^*$ resonance in CO_2. Vertical bars mark the energies at which the Auger electron spectra were measured. The excitations energies for the spectra in Fig. 3 are labeled (A)–(G). (b) Least-squares fit of the residual structure on the high-energy side of the peak after subtracting a broad Voigt profile.

III. RESULTS AND DISCUSSION

A. Total ion yield spectrum

A CO_2 molecule in its electronic ground state, $\ldots 3\sigma_g^2 2\sigma_u^2 4\sigma_g^2 3\sigma_u^2 1\pi_u^4 1\pi_g^4(^1\Sigma_g^+)$, can be resonantly excited to the Renner-Teller split C $1s^{-1}\ \pi_u^*(^1\Pi_u)$ state by a photon of about 290 eV energy. The total ion yield spectrum measured over the C $1s \rightarrow \pi_u^*$ resonance is shown in Fig. 2. The spectrum was taken with 10 meV energy steps at 20 meV photon energy resolution and the energy scale was calibrated using the 290.77 eV peak maximum position from Tronc *et al.* [1]. The overall shape of the resonance can be described by a Voigt profile with 700 meV full width at half maximum (FWHM), although it is slightly asymmetric towards the high photon energy side. This is in general accord with the results of Adachi *et al.* [8], who reported the HWHM of 290 and 350 meV for the lower and higher energy sides of the peak, correspondingly. The low-energy side of the peak is entirely structureless, whereas some weak oscillations can be observed at the high-energy side.

In order to determine the peak positions for these oscillations, a broad Voigt function was first subtracted from the spectrum. The residual signal, shown in Fig. 2(b), was then fit with a manifold of narrower Voigt profiles. During the fitting procedure, the spacing between the peaks was kept equal and a value of 151 meV was obtained for this spacing, with the first peak at 290.86 eV. The structure in Fig. 2(b) is probably due to a vibrational progression. To our knowledge, no calculations of the vibrational energies and potential energy surfaces are available for the C $1s^{-1}\ \pi_u^*$ core-excited state. An estimate for the energies of the vibrational quanta for the C $1s^{-1}\ \pi_u^*$ core-excited states of CO_2 can be obtained, using the $Z+1$ model, from the bent ground electronic state and its linear Renner-Teller split counterpart of

TABLE I. Vibrational characteristics of the ground, core-excited, and final ionic states of CO_2 that are involved in the photoabsorption and Auger decay processes.

	Ground[a]	A_1 [b]	B_1 [b]	$A\ ^2\Pi_u$ [c]
Bond angle (deg.)	180	134	180	180
r_e (Å)	1.160	1.16[d]	1.22[d]	1.224[e]
$\hbar\omega_1$ (meV)	165.3	185.2	156.1	140.0
			151 [d]	
$\hbar\omega_2$ (meV)	82.7	101.7		55.3
$\hbar\omega_3$ (meV)	291.7	239.5	243.2	

[a]Wilson *et al.* [15].
[b]Adachi *et al.* [8], from NO_2 according to the $Z+1$ model. The vibrational energies are mass-corrected where appropriate.
[c]Baltzer *et al.* [12].
[d]This work.
[e]This work, using the valence photoelectron spectrum of Ref. [12].

the NO_2 molecule, based on the $Z+1$ model (see Table I). A comparison to our vibrational spacing of 151 meV suggests that this progression is due to symmetric stretch vibrations of the linear B_1 state. We will return to the assignment of the peaks to specific vibrational levels in conjunction with the analysis of the Auger electron spectra.

B. Resonant Auger electron spectra; general features

The C $1s^{-1}\ \pi_u^*$ core-excited state decays via Auger transitions mainly to the low-energy CO_2^+ states. We measured a series of Auger electron spectra at different photon energies across the C $1s \rightarrow \pi_u^*$ absorption peak, marked by the vertical lines in Fig. 2. A subset of these spectra, taken at the photon energies (A)–(G), is displayed in Fig. 3. In addition, a nonresonant valence photoelectron spectrum (V) taken well below the C $1s^{-1}\ \pi_u^*$ resonance is shown. The binding energy scale of Fig. 3 was calibrated using the average value of 13.787 eV for the two spin-orbit split components of the lowest (000) vibrational level of the ionic $X\ ^2\Pi_g$ state [12]. The binding energy range of Fig. 3 covers the $X\ ^2\Pi_g$, $A\ ^2\Pi_u$, $B\ ^2\Sigma_u^+$, and $C\ ^2\Sigma_g^+$ final states of CO_2^+. Among these, strong resonant enhancement is observed only for the $A\ ^2\Pi_u$ state, which also shows dramatic changes of the vibrational envelope at different photon energies. In contrast, the lowest, $X\ ^2\Pi_g$ state shows only minor changes in the intensity ratios of the vibrational peaks. According to molecular orbital theory, the carbon $2p$ orbital is involved in forming the π_u valence molecular orbital, whereas the π_g orbital is formed only by two oxygen $2p$ orbitals. The overlap of the latter with the carbon $1s$ hole is small and the partial Auger decay rate to the $X\ ^2\Pi_g$ state is thus expected to be low. The resonant behavior of the $B\ ^2\Sigma_u^+$ state is more difficult to determine due to overlap with the higher vibrational levels of the $A\ ^2\Pi_u$ state. Curve fitting results indicate that its behavior is similar to that of the $X\ ^2\Pi_g$ state. In the following analysis, only transitions to the $A\ ^2\Pi_u$ state are considered.

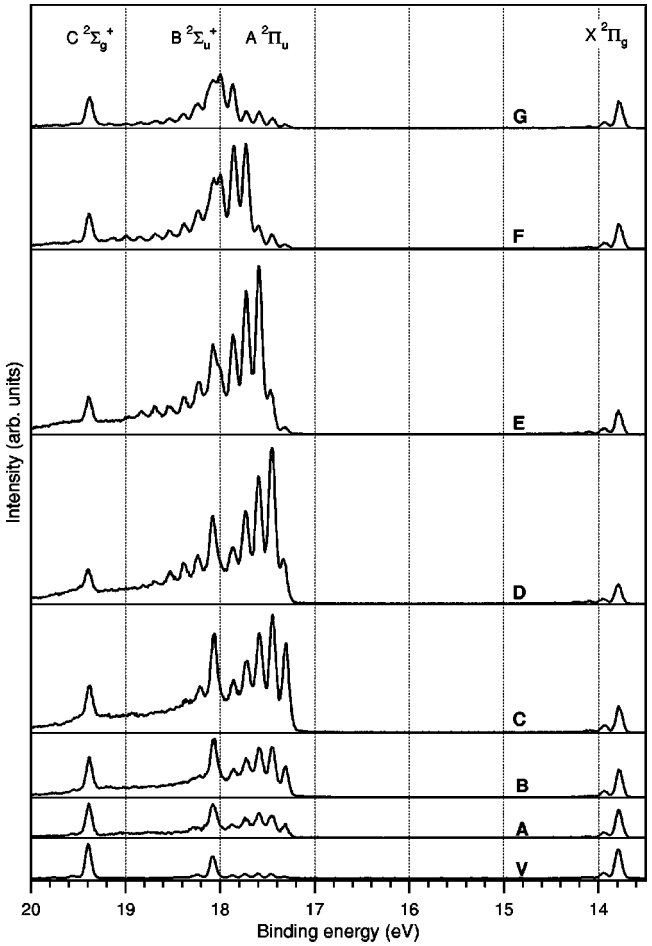

FIG. 3. Resonant Auger electron spectra. Labels refer to the photon energies in Fig. 2. Also shown is a nonresonant valence photoelectron spectrum (V), taken at 280 eV photon energy. The spectral intensities are normalized to the $X\ ^2\Pi_g$ lowest vibrational peak.

A portion of the spectrum (E) from Fig. 3, taken at the peak of the C $1s^{-1}\ \pi_u^*$ resonance, is expanded in Fig. 4. The solid curve through the data points represents a least-squares fit of vibrational peaks to the $A\ ^2\Pi_u$ and $B\ ^2\Sigma_u^+$ bands. The symmetric stretch progression $(v_1 00)$ was found to be the dominant structure in the nonresonant photoelectron spectrum [12] of the $A\ ^2\Pi_u$ state and was included in our fit, with the peak energies fixed to the values given in Ref. [12]. The spin-orbit splitting of the $^2\Pi_u$ state is small (11.8 meV) and the two components were represented by only one peak in our fit. The high-resolution photoelectron spectrum [12] also contains a large number or peaks assigned to the combination bands $(v_1 20)$ with two quanta of the bending mode excited, hot band transitions and vibronic interaction of the electronic state with the bending mode. The $(v_1 20)$ transitions also contribute significantly to the valence photoelectron spectrum [12]. Separation of the $(v_1 20)$ and $(v_1 00)$ series is, however, difficult due to the near degeneracy of the symmetric stretch and bending mode frequencies of the $A\ ^2\Pi_u$ ionic state $(\hbar\omega_1 \approx 2\hbar\omega_2)$. The $(v_1 20)$ transitions were included in the fit with peak energies from Ref. [12]. The intensity ratios $I(v_1 20)/I(v_1 00)$ were kept

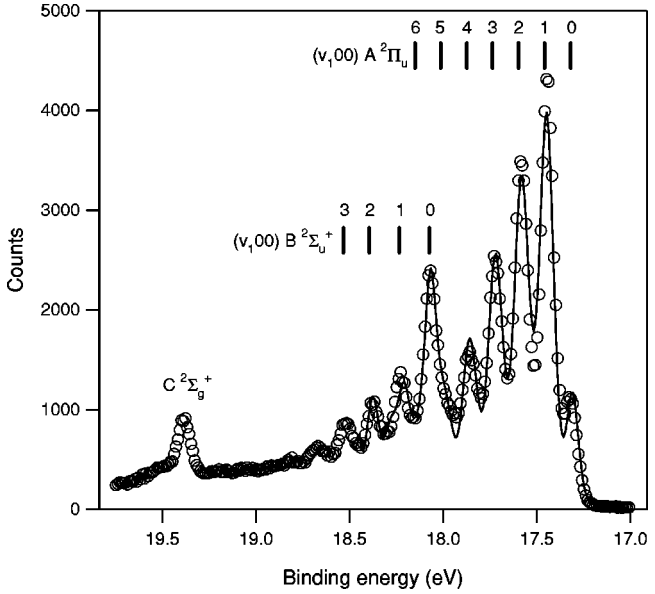

FIG. 4. A least-squares fit of the $A\ ^2\Pi_u$ and $B\ ^2\Sigma_u^+$ states in the Auger electron spectrum (*D*) of Fig. 3.

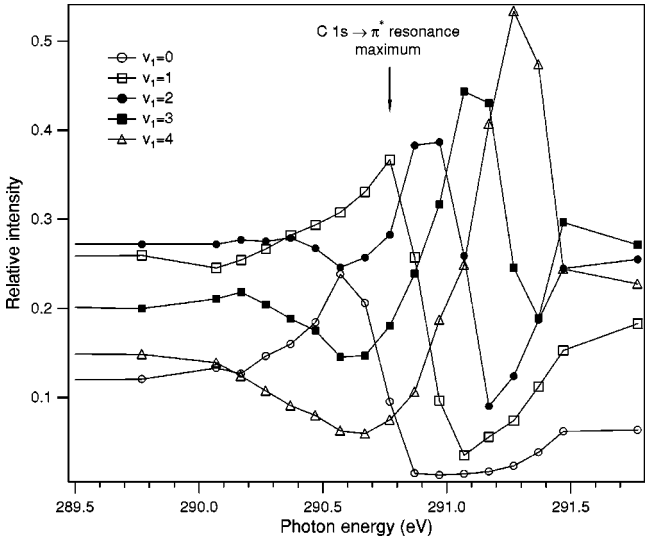

FIG. 5. Relative intensities of the first five peaks of the $A\ ^2\Pi_u$ symmetric stretch progression in the Auger spectra, as a function of photon energy.

equal for all values of v_1. Equal Gaussian linewiths were assigned to the peaks belonging to the same progression. This set of peaks and constraints was found to describe the experimental spectrum adequately, as illustrated by the correspondence of the experimental and modeled spectra in Fig. 4. The main structure of Fig. 4 is assigned to $(v_1 00)A\ ^2\Pi_u$ peaks with the $(v_1 20)$ transitions having considerably less intensity [$<20\%$ of the corresponding $(v_1 00)$ peaks].

The spectrum becomes even more complex above 18 eV binding energy due to overlap with the $B\ ^2\Sigma_u^+$ state. However, the intensity of the (100)+(020) peak of the $B\ ^2\Sigma_u^+$ state is much smaller than that of the ground level (000) peak, which indicates that this vibrational progression decays very rapidly and the structure between 18.5 eV and the onset of the $C\ ^2\Sigma_g^+$ state at about 19.4 eV results from higher vibrational levels of the $A\ ^2\Pi_u$ state. This region of the spectrum shows a smooth, enhanced background, which is apparently a resonant feature, since it is missing in the nonresonant photoelectron spectrum (*V*) of Fig. 3.

As seen from the analysis of the Auger spectrum in Fig. 4, the strongest vibrational structure observed in the Auger spectra can be assigned mainly to the v_1 vibrations of the final ionic state $A\ ^2\Pi_u$, with some contribution from the $(v_1 20)$ combination bands. The relative intensity of the peaks in the $A\ ^2\Pi_u$ band changes dramatically as the photon energy is scanned over the resonance. Figure 5 diplays the relative intensities of the five lowest vibrational levels of the $A\ ^2\Pi_u$ state. The behavior of the vibrational progression changes markedly at about 290.5 eV photon energy. Below that energy, only minor and gradual changes of the intensity distribution occur. Above 290.5 eV, the vibrational structure starts changing rapidly, while the intensity is transferred to the higher members of the series. At even higher photon energies, the intensity distribution again approaches the nonresonant case.

C. Vibrational wave functions and Franck-Condon factors

To complete the vibrational analysis and assignment of the total ion yield and Auger electron spectra, calculated Franck-Condon factors are needed. However, a detailed analysis of vibrational levels, potential energy surfaces, interactions between different vibrational modes and vibronic couplings would be excessive, since such level of detail cannot be obtained from the Auger electron nor the ion yield spectra. We therefore employed a simple model, neglecting interactions between different vibrational modes and between the vibrational and electronic wave functions.

Since both the photoexcitation and Auger decay involve electronic states that have inversion symmetry, excitations of the asymmetric stretch (v_3) mode are assumed to be negligible and will not be considered in our analysis. For the symmetric stretch (v_1) mode, the simplest description is based on the one-dimensional harmonic oscillator model. We used a numerical integration of the Shrödinger equation to obtain energy levels and wave functions, permitting the use of more complex forms of the potential, if needed.

Calculating the wave functions for the bending vibrational mode is a more complicated task, since the model must describe states with linear as well as bent equilibrium geometry. The potential energy curve of the bent core-excited state as a function of the O-C-O angle has a double-well shape and cannot be represented by a quadratic form. Consequently, the motions in the two transverse Cartesian coordinates cannot be separated and the simplest model of doubly degenerate one-dimensional harmonic oscillators is invalid. Therefore, the two-dimensional Shrödinger equation was solved for the bending vibrations in polar coordinates ($x = r\cos\phi, y = r\sin\phi$), where the radial and angular coordinate can be separated for any form of cylindrically symmetric potential. In polar coordinates, the Shrödinger equation has the form

$$\left\{-\frac{\hbar^2}{2m}\left[\frac{1}{r}\frac{\partial}{\partial r}\left(r\frac{\partial}{\partial r}\right)+\frac{1}{r^2}\frac{\partial^2}{\partial\phi^2}\right]+V(r)\right\}u_r(r)u_\phi(\phi)$$
$$=Eu_r(r)u_\phi(\phi), \tag{1}$$

or, after substituting the eigenvalues of the angular momentum operator $-i\hbar(\partial/\partial\phi)$,

$$\left\{-\frac{\hbar^2}{2m}\left[\frac{1}{r}\frac{\partial}{\partial r}\left(r\frac{\partial}{\partial r}\right)\right]+\frac{\hbar^2}{2m}\frac{m_l}{r^2}+V(r)\right\}u_r(r)u_\phi(\phi)$$
$$=Eu_r(r)u_\phi(\phi), \tag{2}$$

where m_l is the angular momentum quantum number. The angular part of the wave function can be easily obtained from Eq. (2) and has the form $u_\phi(\phi)=e^{im_l\phi}$, $m_l=0,\pm1,\pm2,\ldots$. Before solving the radial part of the Shrödinger equation, a substitution $R(r)=r^{1/2}u_r(r)$ was made, so that the radial Shrödinger equation acquires a more convenient form

$$-\frac{\hbar^2}{2m}\frac{d^2R(r)}{dR(r)^2}+\left(\frac{\hbar^2(4m_l^2-1)}{8mr^2}+V(r)\right)R(r)=ER(r). \tag{3}$$

The radial coordinate r corresponds to the distance of the C atom from the line joining the two O atoms and the mass m in Eq. (3) is the reduced mass of the molecule for transverse oscillations

$$m=\frac{2m_Om_C}{2m_O+m_C}. \tag{4}$$

The energies and wave functions were obtained by numerical integration of Eq. (3), adopting a procedure described by Cowan [13]. For the ground state of the CO_2 molecule, using the force constants by Chedin [14], our model yielded $\hbar\omega_2=82.5$ meV, in good agreement with the experimental value of 82.7 meV [15]. A test calculation for bent geometry (ground state of NO_2, using the potential by Tashkun *et al.* [5] shows that our model gives a value for $\hbar\omega_2$ about 25% larger than the accepted value at the bottom of the double well. The discrepancy is probably due to the fact that, if the molecule is regarded as a rigid bender, the O atoms acquire a component of velocity along the O-O line at larger deviations from linear geometry. Equations (1)–(3), however, describe only motions in the transverse plane. Probably the most important simplification of the model is that the coupling between the electronic angular momentum Λ and the angular momentum of the bending vibrations m_l is not taken into account. This coupling results in splitting of energy levels, which are then labeled by the total angular momentum $K=|\pm\Lambda\pm m_l|$, but the influence of this perturbation on the shape of the vibrational wave functions and Franck Condon factors is expected to be minor.

D. Auger decay of the bent core-excited state

1. Symmetric stretch vibrations

The behavior of the vibrational structure in the Auger spectra can be related to the decay of the bent or linear core-excited intermediate states. According to the $Z+1$ analogy, the bent A_1 state is expected to be populated at the lower photon energy side of the absorption peak, while the linear B_1 state becomes accessible only at higher photon energies [4]. This assumption is also supported by recent angle-resolved ion yield measurements [8]. The photon-energy-independent behavior of the vibrational structure in the Auger electron spectrum at lower photon energies therefore reflects the properties of the bent A_1 state. The intensity distribution of the $A^2\Pi_u$ vibrational peaks of the spectra (A)–(C) of Fig. 3 is very similar and does not differ significantly from the intensity distribution in the nonresonant spectrum (V) (see also Fig. 5). This similarity between the resonant and nonresonant spectra indicates that the potential energy surfaces in the coordinate of the symmetric stretch are similar for the linear ground and bent A_1 core-excited states and particularly, that the equilibrium bond lengths of both states must be nearly equal. We can therefore tentatively assign the ground electronic state value $r_e\approx1.16$ Å to the core-excited A_1 state. Consequently, photoabsorption from the ground state excites mainly the lowest vibrational level of the symmetric stretch mode of the A_1 state. The breadth of the absortion profile below the resonance maximum is therefore due to the excitations of other vibrational modes, as discussed below.

2. Bending vibrations

Strong excitation of the bending mode is expected during photoexcitation from the ground state to the A_1 state, since the geometry changes from linear to bent. During the Auger decay from the highly excited bending vibrational levels of the core-excited state, the molecular geometry reverts back to linear. In order to study the v_2 transitions under such circumstances, we have calculated Franck-Condon factors for the photoexcitation and Auger decay. A quadratic form $V(\theta)=\frac{1}{2}f_\theta(\theta-\theta_e)^2$, $\theta_e=180°$ of the potential energy as a function of the bond angle θ was used for the ground and final ionic states, with the vibrational constants $\hbar\omega_2$ as given in Table I. No experimental or theoretical data is available, to our knowledge, about the more complex double-well potential of the A_1 core-excited state. To calculate the energy levels and wave functions for that state, we used the potential energy surface for the ground state of NO_2 by Tashkun and Jensen [5] in the form

$$V(\theta)=\sum_i f^{(i)}(\cos\theta-\cos\theta_e)^i, \tag{5}$$

with the constants $f^{(2)}=9.783$ eV, $f^{(3)}=-10.974$ eV, $f^{(4)}=27.305$ eV, and $\theta_e=133.77°$. The potential energy curves were then converted to the transverse displacement coordinate r for use in Eq. (3) and the bond length of the ground state of CO_2 was used.

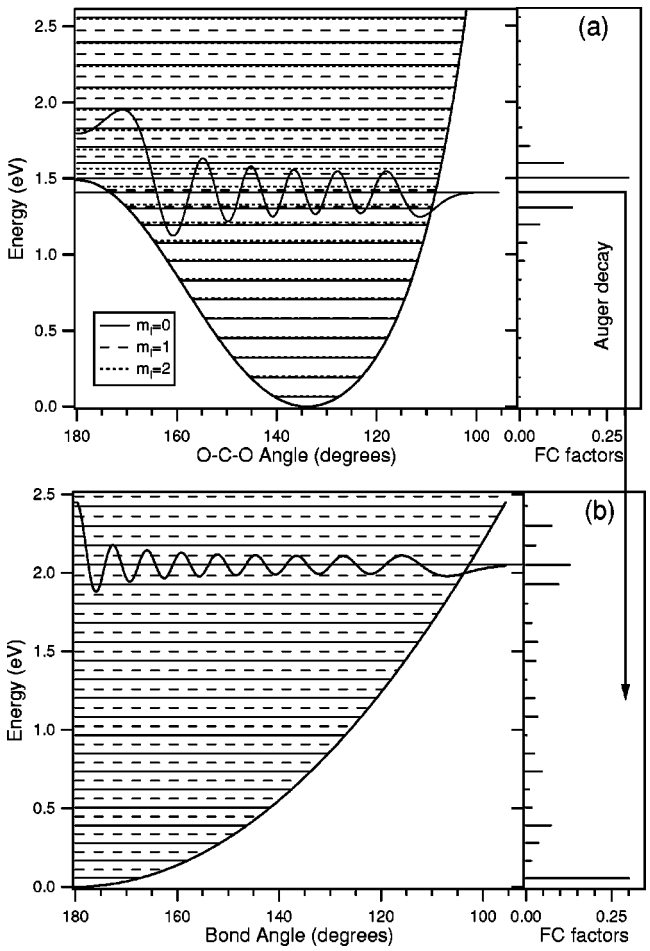

FIG. 6. Potential energy curves along the bond angle of the (a) bent A_1 core-excited state and (b) linear $A\ ^2\Pi_u$ ionic state, together with the energy levels of the bending vibrations. The vibrational wave functions corresponding to some levels are also shown. The right-hand panels display the calculated Franck-Condon factors of the bending mode vibrations for (a) ground-to-A_1 photoexcitation and (b) A_1-to-$A\ ^2\Pi_u$ Auger decay.

The potential energy curve and energy levels for the v_2 vibrations of the A_1 state are shown in Fig. 6(a). The energy levels of the vibrational states with the angular momentum $m_l=0$, 1, and 2 are shown by solid, dashed, and dotted lines, respectively. The states of different angular momentum are degenerate near the bottom of the potential energy well, but this degeneracy is removed near the central maximum, where the wave functions can penetrate through the potential barrier at 180°. Eventually, at still higher energies, the states with $m_l=0$ and 2 again become degenerate, as would be the case for two-dimensional harmonic oscillator. Neglecting vibronic coupling, only transitions to states with $m_l=0$ are allowed from the (000) level of the ground electronic state, which has no angular momentum. However, the states with $m_l=1$ and 2 can become accessible through the coupling of the electronic ($\Lambda=1$ for the $1s^{-1}\pi_u^*$ state) and vibrational angular momenta, and were therefore included in the calculation.

The right-hand panel of Fig. 6(a) shows the calculated Franck-Condon factors for the $(000)\rightarrow(0,v_2^0,0)$ vibrational transitions for the ground electronic state excitations to the A_1 state (superscript denotes the vibrational angular momentum). As an example, a radial wave function of the $v_2=11$ vibrational state is also shown. As expected, only the levels with amplitude near the central maximum have significant overlap with the ground state. The Franck-Condon factors for the higher angular momentum states (not shown in the figure) decrease less rapidly above 1.5 eV than those for the zero-angular-momentum states.

It has therefore been established that only those v_2 energy levels within a range of about 0.5 eV around the central maximum of the potential energy surface of the A_1 state are populated in the photoabsorption and play an important role in the Auger decay. Although we calculated Franck-Condon factors for a large number of C $1s^{-1}\pi_u^*$ $A_1(0,v_2^{m_l},0)$ $\rightarrow A\ ^2\Pi^u(0,v_2^{m_l},0)$ Auger transitions, for clarity only transitions originating from one vibrational level of the core-excited state are shown in Fig. 6(b). The core-excited state vibrational wave functions have the largest overlap with the $v_2=0$ level of the final state. Then follows a range of weakly populated levels until again a considerable overlap occurs with the high-energy levels at around 2 eV above the $v_2=0$ level. This is general behavior of the decay of all vibrational levels of the core-excited state near the central maximum, since large overlap occurs if the classical turning points of both levels match. If the natural broadening of the core-excited state (98 meV [16]) and the finite photon bandwidth (about 75 meV) is taken into account, then it is clear that each Auger electron spectrum originates from several closely spaced vibrational levels of the A_1 state. Since the decay of each of those levels populates strongly the lowest level of the final electronic state, but more weakly the next levels, a distinct v_1 progression, accompanying the transitions to the $v_2=0$ level, should appear in the Auger electron spectra. On the other hand, exactly which high-energy v_2 levels of the final state have the secondary Franck-Condon maximum, depends on the vibrational level of the core-excited state. As each of those transitions is accompanied by its own v_1 progression, the vibrational structure in the high binding energy part of the spectrum becomes unresolved. Furthermore, as shown in a recent theoretical study of the CO_2 ion [17], the higher vibrational levels of the $A\ ^2\Pi_u$ along the bending coordinate are perturbed due to avoided crossing with the $(3)^2\Pi_u$ state. This perturbation can result in a highly irregular congestion of the v_2 levels, which would appear as a continuous background in the electron spectra.

These predictions are indeed supported by the experimental results. The spectra (A)–(C) in Fig. 3 show a well-resolved vibrational structure, assigned to the v_1 progression accompanying the transitions to the $v_2=0$ level, and a high-binding-energy tail that extends to the next $C\ ^2\Sigma_g^+$ band.

The present findings are consistent with the results of electron-ion coincidence measurements [9], where enhanced production of the O^+ ionic fragments was observed at the photon energies below and at the C $1s\rightarrow\pi_u^*$ resonance maximum, as a result of the preferential excitation of the bending mode at these excitation energies.

E. Auger decay of the linear core-excited state

1. Symmetric stretch vibrations

Starting from the photon energies about 300 meV below the peak of the $1s^{-1}\pi_u^*$ resonance, the intensity distribution of the vibrational peaks of the $A\ ^2\Pi_u$ state changes rapidly with the photon energy. We attribute this new behavior to a change over from the decay of the A_1 core-excited state to the decay of the B_1 state. It can be seen from Figs. 3 and 5 that in the spectra (D)–(G) there is a very rapid falloff of the intensity of the vibrational peaks at the low binding energy side of the progression, indicating that the bond lengths of the final ionic and the core-excited B_1 state are similar.

The properties of the potential energy curve for the v_1 vibrations of the $A\ ^2\Pi_u$ Auger final state can be obtained from the high-resolution nonresonant valence photoelectron spectra. We fitted Franck-Condon factors, obtained using a harmonic oscillator potential, to the observed intensities of the $A\ ^2\Pi_u$ photoelectron spectrum [12]. The best fit was obtained at $r_e = 1.224$ Å . This potential energy curve was then used to calculate the Franck-Condon factors for the Auger transitions.

The force constant for the harmonic oscillator potential of the v_1 vibrations of the B_1 state was obtained from the observed splitting of 151 meV from the vibrational structure in the ion yield spectrum, as discussed in Sec. III A. The equilibrium distance of the B_1 state was treated as a free parameter, adjusted to obtain the best match of the Franck-Condon factors with the experiment. The whole vibrational progression in the Auger spectrum is not represented well, since the harmonic oscillator model predicts an equally rapid intensity decrease for the levels both below and above the strongest peak. However, a much slower decrease is observed for the higher vibrational peaks. The discrepancy could be explained by substantial excitations of combination bands involving bending vibrations of the final ionic state. Such transitions are virtually indistinguishable from the pure v_1 transitions due to the degeneracy of the two modes and would appear as intensity enhancement of the higher members of the $(v_1 00)$ series. Secondly, the harmonic oscillator wave functions become increasingly inaccurate for the higher vibrational levels, and using more accurate forms of the potential would probably improve the agreement with the experiment.

The rapid intensity falloff in the low binding energy side of the vibrational envelopes is reproduced well, if the difference between the bond lengths of the core-excited intermediate and final ionic states is about 0.01 Å. Whether the core-excited state has shorter or longer bond length than the final state, cannot be deduced from this calculation. Due to the similar bond lengths, the Franck-Condon overlap is largest between the levels of the same quantum number v_1 in the core-excited and ionic states. For example, the spectrum (D), where the peak with $v_1 = 1$ is the strongest, is mostly due to the decay of the $v_1 = 1$ level of the B_1 state.

The observed spacing between the vibrational peaks in Fig. 2, 151 meV, is comparable with the 98 meV C 1*s* core-hole lifetime in CO_2. Vibrational lifetime interference effects can significantly redistribute the vibrational intensities in the Auger spectra under such conditions [2,3]. We calculated the intensity distributions among the vibrational peaks in the Auger electron spectra with and without the interference terms. While the vibrational lifetime interference has a strong effect on the weaker lines of the spectrum, the main features, such as the location of the strongest line in the vibrational progression, remain unchanged.

The single-hole ionic states populated by participator Auger decay can also be created by the direct (nonresonant) photoionization process. In this case, also, there is interference between the resonant and nonresonant channels, influencing the line shapes and vibrational profiles. Inclusion of such effects requires a knowledge of the amplitudes and phases of the electronic as well as nuclear matrix elements and is beyond the scope of this study. However, a comparison with the the nonresonant spectrum (V) in Fig. 3 shows that the resonant decay channel is the dominant one for the $A\ ^2\Pi_u$ state even at the wings of the absorption profile. The interference effects are thus expected not to have a major influence on the Auger electron spectrum, although they could be responsible for some of the discrepancies between the calculated and observed vibrational profiles.

2. Bending vibrations

Unlike the A_1 state, the photoexcitation and Auger decay of the B_1 state does not involve changes in the equilibrium geometry of the molecule. Therefore, transitions between the lowest levels of the bending vibrations of the ground, core-excited, and final ionic states are expected to prevail. Transitions to higher v_2 levels are possible due to different force constants for the bending vibrations for the different electronic states. However, no reliable values are available for the B_1 core-excited state and thus only a qualitative conclusion that the bending vibrations play a minor role in defining the shape and structure of both the photoabsorption and Auger decay spectra can be drawn.

F. Photoexcitation of the bent and linear core-excited states

The above analysis of the Auger electron spectra provides the modes of vibrational excitations that are expected to build up the absorption profile. In order to test these conclusions, the Franck-Condon factors for photoexcitation from the ground to C $1s^{-1}\pi_u^*$ states were calculated and compared with the measured ion yield profile. Figure 7 displays the total ion yield spectrum together with the calculated Franck-Condon factors for the v_2 excitations of the A_1 state and v_1 excitations of the B_1 state. The v_1 excitations of the A_1 state and v_2 excitations of the B_1 state were not included in the calculation, since they are expected to be of lesser intensity and also because the available information about the potential energy surfaces of these states is insufficient in these dimensions. The energies of the v_1 excitations of the A_1 state were determined from the fit of the vibrational structure of Fig. 2(b). According to the assignment based on the Auger electron spectra, the first fitted peak corresponds to the $v_1 = 2$ level of A_1 state. The first two peaks of the series were not fitted, since such weak intensity oscillations could not be observed near the maximum of the main peak, where the curvature of the absorption profile is large. This assign-

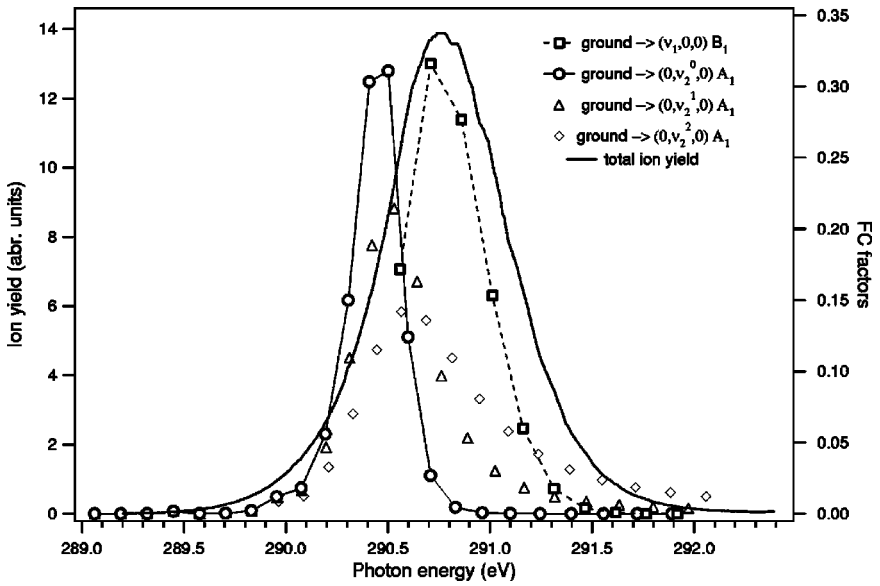

FIG. 7. Total ion yield spectrum over the carbon $1s\rightarrow\pi_u^*$ resonance, together with calculated Franck-Condon factors.

ment places the (000) level of the B_1 state at 290.56 eV. In order to find the minimum of the potential energy surface, the value of $\hbar\omega_2$ is needed for that state. For an estimate, we used the value of 82 meV from the ground state, which gives the minimum of the potential energy surface of the B_1 state $[E_{B_1,el}=E_{B_1}(000)-\frac{1}{2}\hbar\omega_1-\hbar\omega_2]$ at 290.40 eV above the (000) level of the ground state.

At this energy, the bottom of the potential energy surface of the B_1 state meets the central maximum of the double-well potential energy surface of the A_1 state. The energies of the v_2 vibrational levels of the A_1 state were thus determined by placing the central maximum of our potential energy curve in the bending coordinate at 290.40 eV above the (000) level of the ground state and adding $\frac{1}{2}\hbar\omega_1$ to account for the zero-level energy of the v_1 vibrations.

Franck-Condon factors for the v_1 excitations of the B_1 state were calculated using harmonic oscillator potentials for both the ground and excited states, with the parameters given in Table I. For the v_2 excitations of the A_1 state, a harmonic oscillator potential was used for the ground state and the double-well potential [Fig. 6(a)] for the excited state. The vibrational wave function overlap with the (000) level of the ground electronic state was calculated in the radial (r) coordinate for the angular momentum states $m_l=0,1,2$. Although the overlap of the angular part of the wave functions is zero in the ϕ coordinate for $m_l>0$, coupling of the electronic and vibrational angular momenta can make these states available. The Franck-Condon factors for the $m_l=1,2$ states are also shown in Fig. 7, assuming that the selection rule $\Delta m_l=0$ is broken by vibronic coupling. Note that the relative strengths of the $m_l=0$, 1, and 2 envelopes is not accurately represented, since it is determined by the strength of the vibronic coupling, which is not evaluated here.

The calculated Franck-Condon factors represent the general shape and width of the absorption profile in Fig. 7, although there is an offset of the calculation towards lower photon energy. This is probably due to a number of approximations in our simulation. Most importantly, simultaneous excitations of the v_1 and v_2 modes are not accounted for. A convolution of the calculated (v_100) and $(0,v_2^0,0)$ Franck-Condon factors with a 98-meV Lorentzian and 20-meV Gaussian representing experimental resolution still shows clearly resolved peaks for the (v_100) progression of the B_1 state. The less resolved experimental result suggests the presence of additional vibrational transitions such as combination bands.

IV. CONCLUSIONS

The carbon $1s\rightarrow\pi_u^*$ core excitations in the CO_2 molecule decay mainly via participator Auger transitions to the $A\ ^2\Pi_u$ ionic state. The vibrational structure of the Auger electron spectra is sensitive to the excitation energy. In particular, the decay of the bent A_1 and linear B_1 Renner-Teller split components of the C $1s^{-1}\pi_u^*$ state produces clearly different vibrational patterns. It was concluded from the analysis of the Auger electron spectra that high levels of the bending vibrations of the A_1 state are excited in photoabsorption and the symmetric stretch excitations play only a minor role. In contrast, higher levels of symmetric stretch vibrations can be excited in the photoabsorption to the B_1 component, for which the bending mode excitations are much less important. The photon energy-dependent features in the resonant Auger spectra were explained using these main characteristics of the core excitations.

We calculated Franck-Condon factors for the relevant vibrational transitions and estimated the equilibrium bonds lengths of the A_1 and B_1 states. Indications of a vibrational progression, seen on the high-energy side of the absorption profile, were fitted and, using the Auger electron spectra, assigned to the symmetric stretch vibrations of the B_1 state. The energy of the carbon $1s\rightarrow\pi_u^*$ electronic excitation was estimated for the linear geometry of the molecule, where the two Renner-Teller split states are degenerate, to be 290.4 eV above the (000) level of the ground electronic state.

Photon-energy-dependent Auger electron spectra provide a considerably more detailed view into the core-excitation process of CO_2 than can be obtained from the photoabsorp-

tion spectra. Vibrational structure of core excitations as well as properties of the potential energy surfaces of larger molecules can be studied with the help of Auger electron spectroscopy. While the present study addresses the main features of the photoexcitation and Auger decay in a triatomic molecule, advanced calculations of the electronic and vibrational properties of the core-excited states would be needed for further analysis.

ACKNOWLEDGMENTS

This work was supported by the Department of Energy, Office of Science, Basic Energy Sciences, Chemical Sciences Division. The Advanced Light Source is supported by the Department of Energy, Materials Sciences Division. We are thankful to Dr. Leif Sæthre for reading and commenting on the manuscript.

[1] M. Tronc, G.C. King, and F.R. Read, J. Phys. B **12**, 137 (1979).
[2] S.J. Osborne, A. Ausmees, S. Svensson, A. Kivimäki, O.-P. Sairanen, A. Naves de Brito, H. Aksela, and S. Aksela, J. Chem. Phys. **102**, 7317 (1995).
[3] E. Kukk, J.D. Bozek, W.-T. Cheng, R.F. Fink, A.A. Wills, and N. Berrah, J. Chem. Phys. **111**, 9642 (1999).
[4] G.R. Wight and C.E. Brion, J. Electron Spectrosc. Relat. Phenom. **3**, 191 (1973).
[5] S.A. Tashkun and P. Jensen, J. Mol. Spectrosc. **165**, 173 (1994).
[6] G. Hertzberg and E. Teller, J. Phys. Chem. B **21**, 410 (1933).
[7] R. Renner, J. Phys. Chem. B **38**, 381 (1934).
[8] J. Adachi, N. Kosugi, E. Shigemasa, and A. Yagishita, J. Chem. Phys. **107**, 4919 (1997).
[9] P. Morin, M. Simon, C. Miron, N. Leclercq, E. Kukk, J.D. Bozek, and N. Berrah, Phys. Rev. A **61**, 050701 (2000).
[10] N. Berrah, B. Langer, A.A. Wills, E. Kukk, J.D. Bozek, A. Farhat, and T.W. Gorczyca, J. Electron Spectrosc. Relat. Phenom. **101**, 1 (1999).
[11] P. Baltzer, L. Karlsson, M. Lundqvist, and B. Wannberg, Rev. Sci. Instrum. **64**, 2179 (1993).
[12] P. Baltzer, F.T. Chau, J.H.D. Eland, L. Karlsson, M. Lundqvist, J. Rostas, K.Y. Tam, H. Veenhuizen, and B. Wannberg, J. Chem. Phys. **104**, 8922 (1996).
[13] R.D. Cowan, *The Theory of Atomic Structure and Spectra* (University of California Press, Berkeley, 1981).
[14] A. Chedin, J. Mol. Spectrosc. **76**, 430 (1979).
[15] E.B. Wilson, J.C. Decius, and P.C. Cross, *Molecular Vibrations: the Theory of Infrared and Raman Vibrational Spectra* (Dover Publications, New York, 1980).
[16] T.X. Carroll, J. Hahne, T.D. Thomas, L.J. Saethre, N. Berrah, J. Bozek, and E. Kukk, Phys. Rev. A **61**, 042503 (2000).
[17] R. Polak, M. Hochlaf, M. Levinas, G. Chambaud, and P. Rosmus, Spectrochim. Acta A **55**, 447 (1999).